Sea Surface Temperatures Derived From COCTS Onboard the HY-1C Satellite

Xiaomin Ye, Jianqiang Liu, Mingsen Lin, *Member, IEEE*, Jing Ding, Bin Zou, and Qingjun Song

***Abstract*—As one of the key payloads onboard the HY-1C satellite, the Chinese ocean color and temperature scanner (COCTS) was designed for global sea surface temperature (SST) and ocean color detection. In this study, a nonlinear SST algorithm (NLSST) is applied to derive SSTs from the brightness temperatures (BTs) of the two COCTS thermal infrared bands at 10.8 and 12.0 μm. The SST retrieval results from the multichannel SST algorithm (MCSST) are used as the first guess for the input of the NLSST algorithm. The coefficients of both the MCSST and NLSST algorithms are regressed from the matchup datasets of the COCTS BT observations and the measurements from the *in situ* quality monitor system (iQuam), which were collected from September 10 to December 31, 2018. The retrieval SSTs from January 1, 2019 to March 31, 2020 are evaluated by the *in situ* measurements from iQuam with root mean square errors of 0.84 °C for daytime and 0.97 °C for nighttime and robust standard deviations (RSDs) of 0.73 °C for daytime and 0.72 °C for nighttime. Daily gridded retrieval SSTs from September 10, 2018 to March 31, 2020 are compared with SSTs from moderate-resolution imaging spectroradiometer (MODIS) onboard Terra satellite. The cross comparison RSDs are 0.56 $\pm$ 0.05 °C for daytime and 0.67 $\pm$ 0.05 °C for nighttime.**

***Index Terms*—Chinese ocean color and temperature scanner (COCTS), HY-1C satellite, nonlinear SST algorithm (NLSST), sea surface temperature (SST).**

I. Introduction

SEA surface temperature (SST) is an important measurement for ocean, weather, and climate and can be applied in numerical ocean and atmospheric models, fishery science, and for tactical support of commercial fishing activities, physical oceanographic research, and climate monitoring [1]–[7]. SST can be obtained by space-borne microwave radiometers, infrared (IR) radiometers, buoys, and ships. Buoys and ships measure the water "bulk" temperature at particular points, whereas satellite radiometers continuously measure SST over global water surfaces with a spatial scale of one kilometer to tens of kilometers [8].

Satellite measurements of SST began in the 1970s using IR radiometers onboard the geostationary and polar orbiting platforms of the National Ocean and Atmospheric Administration (NOAA) [9], [10]. IR radiometers, such as the advanced very high resolution radiometer (AVHRR), moderate-resolution imaging spectroradiometer (MODIS), sea and land surface temperature radiometer (SLSTR), and visible infrared imaging radiometer (VIIRS), have been providing global SSTs for more than 40 years. Although the microwave radiometer can measure the sea surface through clouds under all weather conditions except rain, the IR SSTs have a higher resolution ($\sim$1 km) than microwave SSTs ($\sim$25 km). For the IR radiometers, the SSTs are retrieved from brightness temperatures (BTs) of thermal infrared (TIR) bands at 11 and 12 μm or the TIR bands combined with the mid-IR band (e.g., at 3.7 μm for VIIRS). The retrieval algorithms can be split-window algorithms [e.g., multichannel SST algorithm (MCSST) [10]; nonlinear SST algorithm (NLSST) [1]], physical retrievals based on radiative transfer model simulations [12], [13], and neural network models [14]. The SST retrieval algorithm can be developed for the global ocean [13], [16]–[18] or for regional marine waters [19], [20].

China launched the ocean satellite Haiyang-1C (HY-1C) on September 7, 2018, which is equipped with the Chinese ocean color and temperature scanner (COCTS), a multispectral radiation sensor that can monitor global ocean color and surface temperature every day. As a member of the space-borne sensor designed for global ocean color and SST monitoring, the performance of this sensor should be evaluated. In this study, the SSTs of COCTS onboard HY-1C (COCTS/HY-1C) are processed by the NLSST algorithm with the regression coefficients from matchups between the satellite observations and *in situ* measurements. The SST retrieval results are evaluated by comparison with both *in situ* data and MODIS SST products. This study is outlined as follows. Section II introduces the description of COCTS/HY-1C and its data. Section III introduces the methodology, including the method of the SST retrieval algorithm and clear-sky mask proceeding for COCTS. Section IV presents the retrieval results of SST from COCTS and their evaluation against both *in situ* and MODIS data. Finally, the discussions and conclusions are presented in Sections V and VI.

II. Data and Description of COCTS

The Chinese HY-1C satellite, the follow-on mission to the HY-1A and HY-1B satellites, was launched on September 7, 2018. This satellite is equipped with the COCTS and a coastal zone imager, as well as an ultraviolet imager, a satellite calibration spectrometer, and a satellite-based automatic identification

Manuscript received June 30, 2020; revised September 17, 2020; accepted October 13, 2020. Date of publication October 23, 2020; date of current version January 6, 2021. This work was supported in part by the National Key Research and Development Program of China under Grant 2016YFB0500502 and in part by the National Natural Science Foundation of China under Grant 41876211, Grant 41876204, and Grant 41506206. *(Corresponding author: Mingsen Lin.)*

The authors are with the National Satellite Ocean Application Service, Beijing 100081, China, and also with the Key Laboratory of Space Ocean Remote Sensing and Application, Ministry of Natural Resources, Beijing 100081, China (e-mail: yexiaomin2011@foxmail.com; jqliu@mail.nsoas.org.cn; mslin@mail.nsoas.org.cn; dingjing@mail.nsoas.org.cn; zoubin@mail.nsoas.org.cn; kingdream@mail.nsoas.org.cn).

Digital Object Identifier 10.1109/JSTARS.2020.3033317

TABLE I
SPECIFICATIONS OF COCTS/HY-1C

Band No.	Spectral Range (μm)	Central Wavelength	SNR or NEΔT @ Specified Input (Measurement Condition)	Maximal Radiance ($mW \cdot cm^{-2} \cdot \mu m^{-1} \cdot Sr^{-1}$)
1	0.402-0.422	412 nm	349 @ 9.10 $mW \cdot cm^{-2} \cdot \mu m^{-1} \cdot Sr^{-1}$	13.94
2	0.433-0.453	443 nm	472 @ 8.41 $mW \cdot cm^{-2} \cdot \mu m^{-1} \cdot Sr^{-1}$	14.49
3	0.480-0.500	490 nm	467 @ 6.56 $mW \cdot cm^{-2} \cdot \mu m^{-1} \cdot Sr^{-1}$	14.59
4	0.510-0.530	520 nm	448 @ 5.46 $mW \cdot cm^{-2} \cdot \mu m^{-1} \cdot Sr^{-1}$	13.86
5	0.555-0.575	565 nm	417 @ 4.57 $mW \cdot cm^{-2} \cdot \mu m^{-1} \cdot Sr^{-1}$	13.89
6	0.660-0.680	670 nm	309 @ 2.46 $mW \cdot cm^{-2} \cdot \mu m^{-1} \cdot Sr^{-1}$	11.95
7	0.730-0.770	750 nm	319 @ 1.61 $mW \cdot cm^{-2} \cdot \mu m^{-1} \cdot Sr^{-1}$	9.72/5.0*
8	0.845-0.885	865 nm	327 @ 1.09 $mW \cdot cm^{-2} \cdot \mu m^{-1} \cdot Sr^{-1}$	6.93/3.5*
9	10.30-11.30	10.8 μm	0.20 @ 300 K	200-320 K**
10	11.50-12.50	12.0 μm	0.20 @ 300 K	200-320 K**

*Two possible settings; the lower one is the default.
**The range of brightness temperature.

TABLE II
COEFFICIENTS OF SST RETRIEVAL ALGORITHMS OF COCTS/HY-1C

Algorithm	a_0	a_1	a_2	a_3	a_4	a_5	a_6
NLSST (Daytime)	-262.261	0.956630	0.010960	0.077157	0.055268	0.633974	-2.385393
NLSST (Nighttime)	-261.142	0.948632	0.028582	0.844316	0.048282	0.202644	-6.541562
—	b_0	b_1	b_2	b_3	—	—	—
MCSST (Daytime)	-280.823	1.022991	0.995850	1.075705	—	—	—
MCSST (Nighttime)	-283.564	1.033302	0.868894	1.106714	—	—	—

system receiver. The orbit altitude and tilting angle are 782 km and 98.5°, respectively. The overpass time is 10:30 A.M. ± 30 min local time at the descending node.

The COCTS is a moderate-resolution imaging scanner with a nadir spatial resolution of 1.1 km and a viewing swath width of more than 2900 km. The satellite measures signals in eight visible and near-infrared bands and two TIR bands. The objective of the COCTS is global ocean color and SST monitoring for the routine operational application and study of biological oceanography, marine ecological protection, marine disaster prevention, and climate change. The COCTS can also be used to observe sea ice, shallow sea terrain, ocean current characteristics, and atmospheric aerosols on the sea surface and for terrestrial natural resource research and investigation. COCTS detects the global ocean and land twice a day and provides daily ocean color, land vegetation products, and daytime and nighttime SST. Spectral specifications (spectral range, central wavelength, signal-to-noise ratio (SNR), noise-equivalent change in temperature (NEΔT), maximal radiance, and observation objective) of COCTS/HY-1C are detailed in Table I.

HY-1C satellite data are received by the ground receiving stations of the National Satellite Ocean Application Service (NSOAS) of the Ministry of Natural Resources of China. HY-1C can provide near real-time observation data for China's coastal regions. The remote sensing data covering the rest of the Earth are stored in the onboard data storage device for delayed replay. HY-1C products are available free to the public from the Ocean Satellite Data Distribution System (OSDDS) of NSOAS. The BT data used in this study are derived from the level 1B (L1B) standard product of COCTS and provided by OSDDS. The L1B data of COCTS are the calibrated radiances of 10 bands with geolocation [21].

TABLE III
TESTS AND THEIR THRESHOLDS FOR CLEAR-SKY MASKS OF COCTS/HY-1C

Tests	**Thresholds for clear-sky**
T11 Gross Cloud	270 K $\leq T_{12} \leq$ 310 K
T12 Gross Cloud	268 K $\leq T_{12} \leq$ 310 K
SST Uniformity	std[SST(5×5 pixels)]≤1 °C
Unreasonable SST	-2℃ ≤ SST ≤ 35 °C
Climatology	$\lvert SST\text{-}SST_{clim} \rvert \leq$ 10 °C

III. METHODOLOGY

A. Retrieval Algorithm of SST

The SST retrieval algorithms used in this study are the modified version of the NLSST of Walton *et al.* [1]. The NLSST algorithm for the two TIR bands of COCTS can be described as follows:

$$\begin{aligned} \mathrm{SST} &= a_0 + (a_1 + a_2 S_\theta) T_{11} \\ &\quad + [a_3 + a_4 T_{\mathrm{sfc}} + a_5 S_\theta](T_{11} - T_{12}) + a_6 S_\theta, \end{aligned} \quad (1)$$

where $S_\theta = \sec_\theta - 1$ and θ is the sensor zenith angle, T_{11} and T_{12} are the BTs of the TIR bands of COCTS at 10.8 and 12.0 μm, respectively, $a_0 - a_6$ are the algorithm coefficients, and T_{sfc} is the

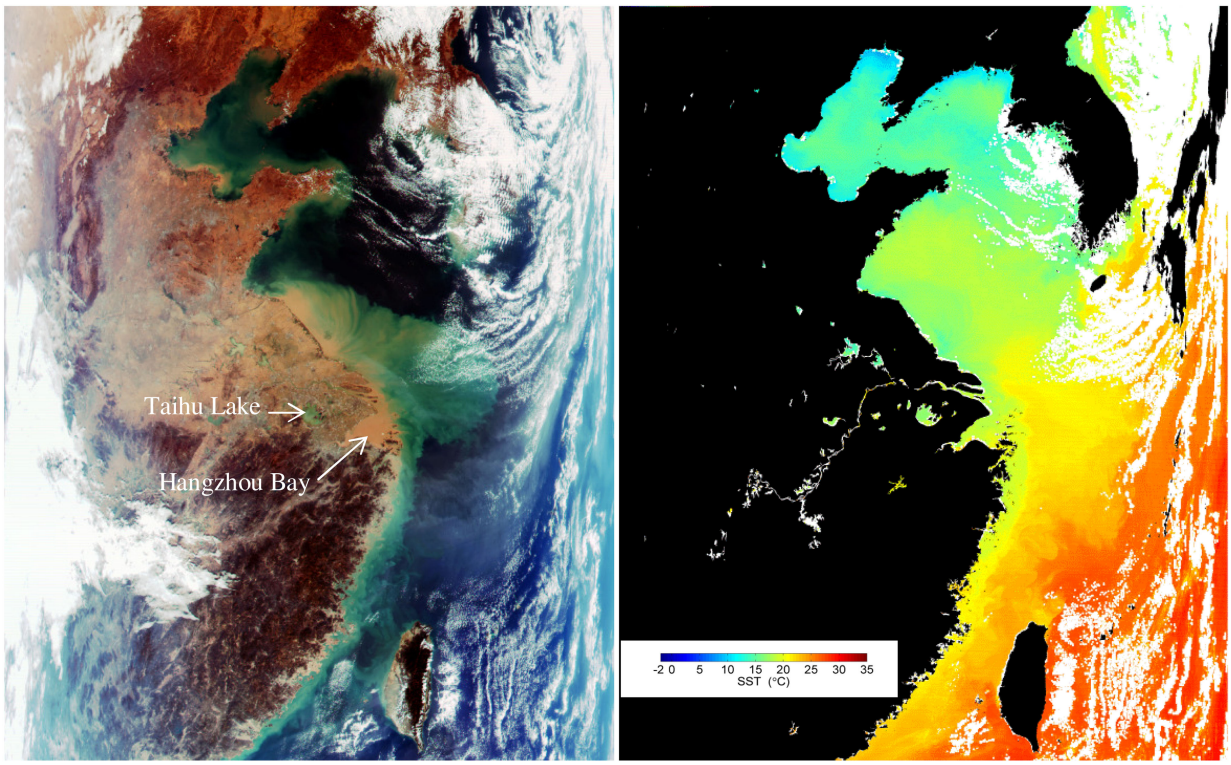

(a) (b)

Fig. 1. COCTS/HY-1C data covering China's east coastal region acquired at 02:53 UTC on November 11, 2019 for (a) true color image and (b) its SST retrieval results.

reference SST used as the first guess. In this study, $T_{\rm sfc}$ is derived from COCTS by a MCSST. The equation form of MCSST is described as follows [10]:

$$\begin{aligned} \mathrm{SST} = {} & \mathrm{b}_0 + \mathrm{b}_1 T_{11} + \mathrm{b}_2 (T_{11} - T_{12}) \\ & + \mathrm{b}_3 (T_{11} - T_{12}) S_\theta, \end{aligned} \tag{2}$$

where $\mathrm{b}_0 - \mathrm{b}_3$ are the algorithm coefficients of MCSST for COCTS. Their values in both formulas (1) and (2) are derived by regression of collocated *in situ* SSTs and HY-1C satellite-observed BTs of T_{11} and T_{12}.

The signals received by the satellite TIR sensor are the emissions formed in the top $\sim 10-20$ μm of water and are sensitive to the so-called "skin" SST [22], [23]. The *in situ* SSTs, however, are the "bulk" SSTs, which may differ from "skin" SSTs due to the skin effect [22]. The satellite-observed BTs, from which the SSTs are derived, are sensitive to water skin ($\sim 10-20$ μm) temperature. Therefore, the SST retrieved here reflects variations in water skin temperature but represents water bulk temperature on average [22]. The regression method was also applied in MODIS and VIIRS [13], [15], [16], [24], [25].

The *in situ* SSTs used in this study are the water bulk temperatures from the *in situ* quality monitor system (iQuam; available, at[1]) developed by the Center for Satellite Applications and Research (STAR), National Oceanic and Atmospheric Administration (NOAA) Satellite and Information Service (NESDIS) [26]. Only the iQuam dataset with the highest quality (i.e., the quality flags of 5 in the dataset) and measured at a water depth of less than 1 m are used. The coefficients of the SST retrieval algorithms were regressed from 862 and 507 matchups collected from September 10 to December 31, 2018 during daytime and nighttime, respectively. The time interval between *in situ* and satellite measurements is $\leq$2 h, and the distances between the locations of *in situ* measurements and the nearest clear-sky pixel are $\leq$10 km. The obtained coefficients for formulas (1) and (2) of COCTS/HY-1C are detailed in Table II.

The coefficients detailed in Table II for daytime and nighttime are different from each other, and this difference is because they are regressed by daytime and nighttime datasets, respectively. Therefore, they are separately applied in SST retrieval for COCTS in daytime and nighttime. By using the algorithm coefficients in Table II, the input data of T_{11} and T_{12} are in units of Kelvins, and the SST output for both the MCSST and NLSST algorithms are in units of degrees centigrade (°C).

B. Clear-Sky Mask

The SST retrieval from TIR BT data should be processed from clear-sky water with no sea ice or snow. Thus, some cloud and sea snow/ice detection tests with their thresholds are used to detect these ideal situations. Table III lists the tests and thresholds for the clear-sky mask used in this study.

For the daytime data, the criteria of $\rho_{865} \geq 0.20$ and $\rho_{412} \geq 0.35$ are also used to detect the clouds and sea ice/snow pixels,

[1][Online]. Available: www.star.nesdis.noaa.gov/sod/sst/iquam/

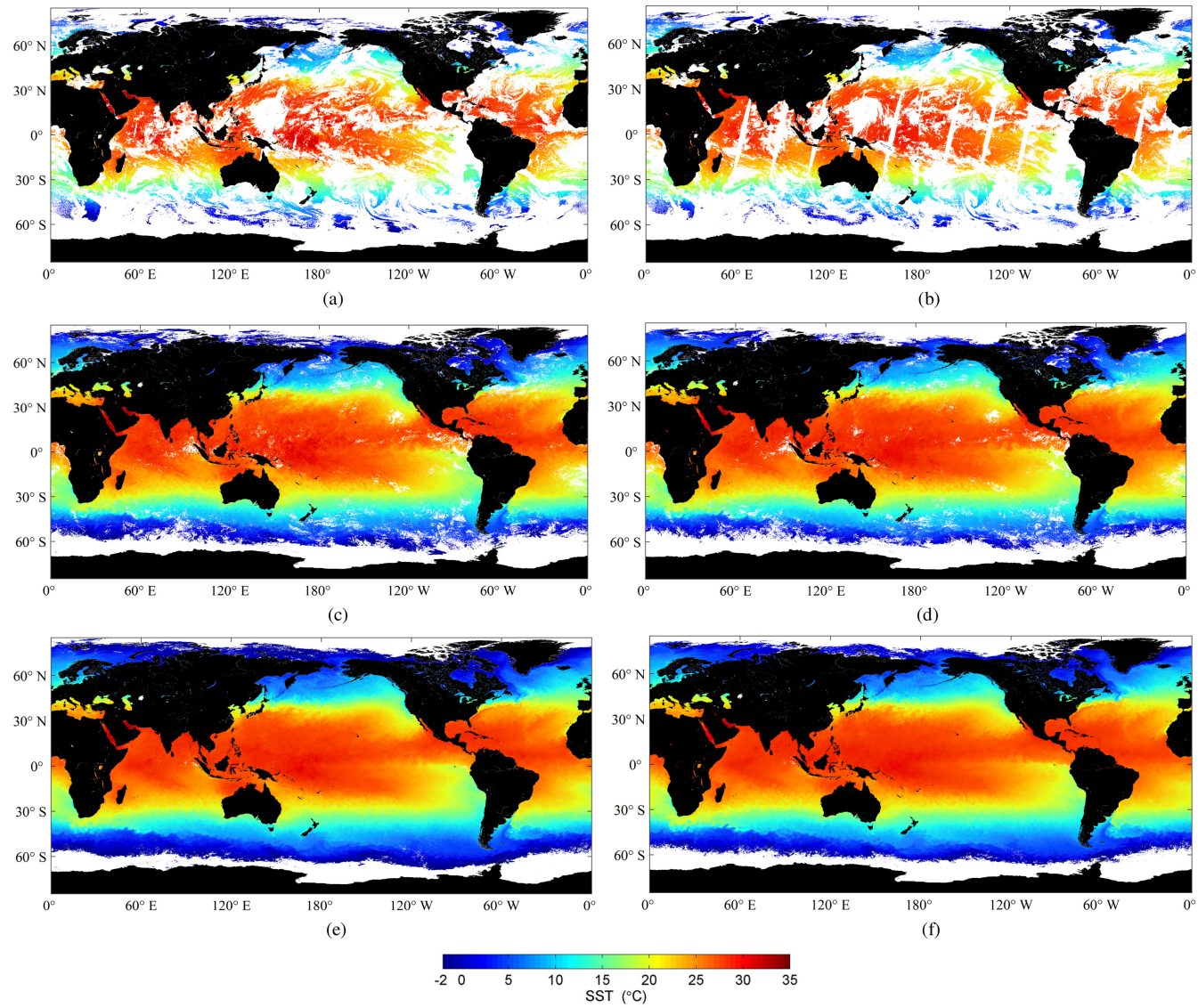

Fig. 2. Daytime SST derived from COCTS/HY-1C and MODIS/Terra. (a) Daily (October 8, 2019), COCTS/HY-1C. (b) Daily (October 8, 2019), MODIS/Terra. (c) Eight-day (October 8−15, 2019), COCTS/HY-1C. (d) Eight-day (October 8−15, 2019), MODIS/Terra. (e) Monthly (October 2019), COCTS/HY-1C. (f) Monthly (October 2019), MODIS/Terra.

where ρ_{412} and ρ_{865} are the reflectance of the visible bands of COCTS at the wavelengths of 412 and 865 nm, respectively. $\rho_\lambda = \pi L_{t\lambda}/F_{0\lambda}\cos\theta_0$ is the reflectance at the wavelength of λ. L_t, F_0, and θ_0 are the radiance, the extra-terrestrial solar constant adjusted by the spectral channel response function of COCTS, and the zenith angle of the solar radiation, respectively. The subscripts λ are the wavelengths in units of nm. The contiguous cloudy pixels are masked as probably cloudy, which are not treated as clear-sky pixels.

IV. Results and Evaluation

A. SST Retrieval Results

By using the method and data process of SST retrieval in the above section, the SSTs are derived from the TIR BTs of COCTS. Fig. 1 presents an example of a remote sensing image covering China's east coastal water area from 18.5 °N to 43.8 °N and 102.5 °E to 140.0 °E and its retrieval results from the COCTS as a case study, which was acquired on November 11, 2019 at the imaging central time of 02:53 UTC.

Fig. 1(a) is the true color image composited by radiances of Band-6, Band-4, and Band-2 of COCTS. The color-coded region in Fig. 1(b) is the SST retrieval result derived from the data shown in Fig. 1(a). A comparison of the image shown in Fig. 1(a) with the SST shown in Fig. 1(b) clearly shows that the clear-sky water pixels, including the highly turbid water and some inland water of lakes, e.g., the water in Hangzhou Bay and Taihu Lake, are successfully detected and retrieved for SST.

For the L1B data of COCTS/HY-1C used in this study, the length of observation time for every data file is approximately 5 min. A global SST mapped product can be temporally and spatially aggregated onto a georeferenced Earth grid over a

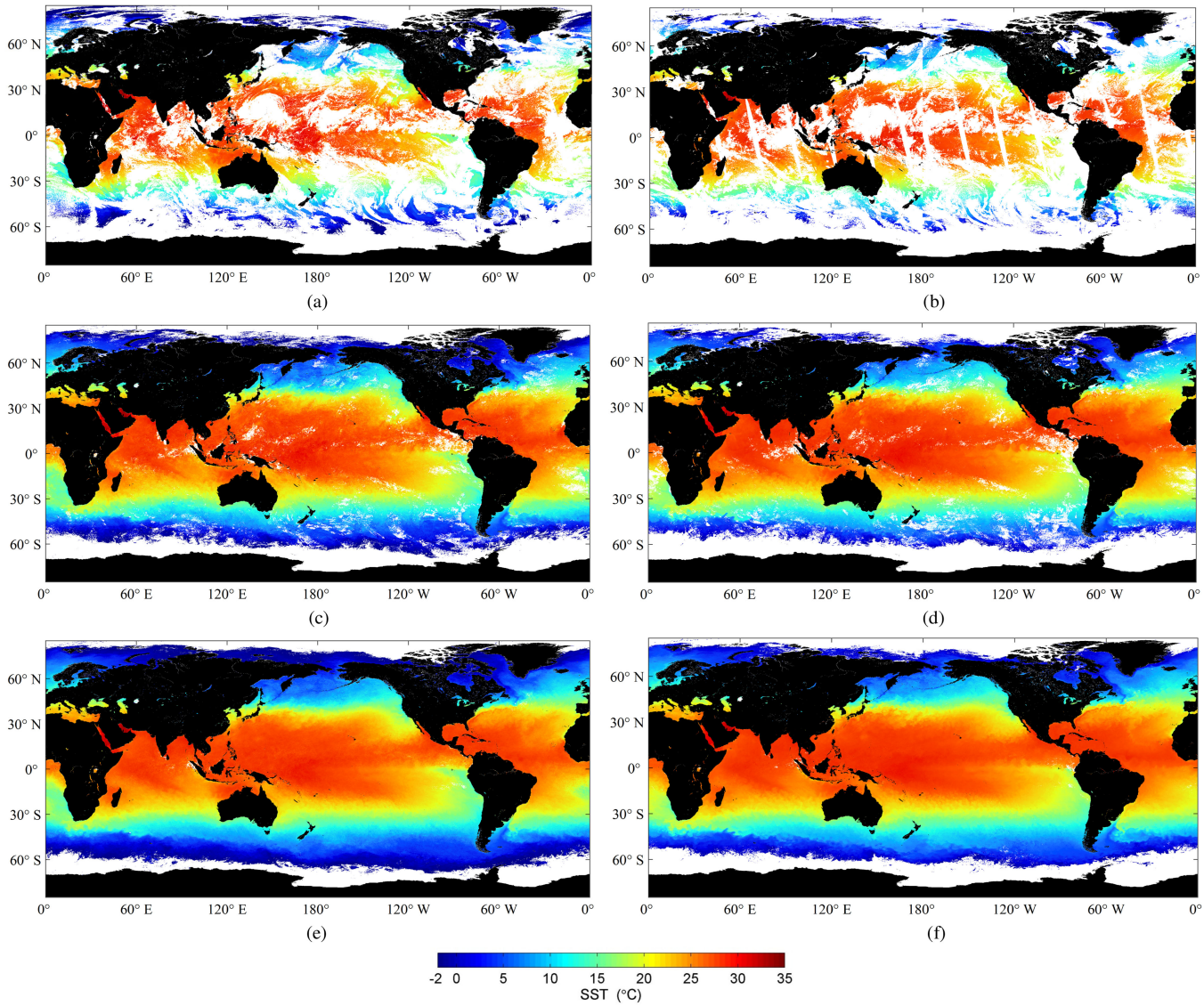

Fig. 3. Nighttime SST derived from COCTS/HY-1C and MODIS/Terra. (a) Daily (October 8, 2019), COCTS/HY-1C. (b) Daily (October 8, 2019), MODIS/Terra. (c) Eight-day (October 8−15, 2019), COCTS/HY-1C. (d) Eight-day (October 8−15, 2019), MODIS/Terra. (e) Monthly (October 2019), COCTS/HY-1C. (f) Monthly (October 2019), MODIS/Terra.

defined period by a binning algorithm [27]. In this study, global ocean SST maps were created with a grid size of 9.2 km and periods of one day, eight days, a calendar month, a calendar season, and a calendar year and then georeferenced onto a Plate Carrée projection. Because they have the same gridded size and period as NASA's standard map (L3M) SST product, the global SST products from COCTS/HY-1C are compared with MODIS L3M products to evaluate their performance.

Figs. 2 and 3 present examples of the daily, eight-day, and monthly global gridded daytime and nighttime SST maps from COCTS, respectively. The same kind of SST maps from MODIS onboard Terra (MODIS/Terra) are also presented in Figs. 2 and 3 for comparison. The MODIS/Terra data were selected for comparison because they have almost the same overpass time as the descending and ascending nodes.

The gaps in Figs. 2(b) and 3(b) are water areas that could not be covered by MODIS in one day. As the SST distribution maps in Figs. 2(a) and 3(a) show, in a period of one day, the COCTS can cover the whole global ocean with no gaps regardless of cloud or sea ice/snow coverage. A comparison of the distribution maps of COCTS with those of MODIS shown in Figs. 2 and 3 shows a lack of large SST difference between the two space-borne sensors.

B. *Evaluation of SST*

To quantitatively evaluate the SST derived from COCTS/HY-1C and the consistency of SST from COCTS/HY-1C and MODIS/Terra, the mean bias, standard deviation (SD), root mean square error (RMSE), median, and robust standard deviation (RSD) are used in this study to describe the differences between the SSTs from COCTS and *in situ* and MODIS measurements. The statistics used can also be found in [28]−[31].

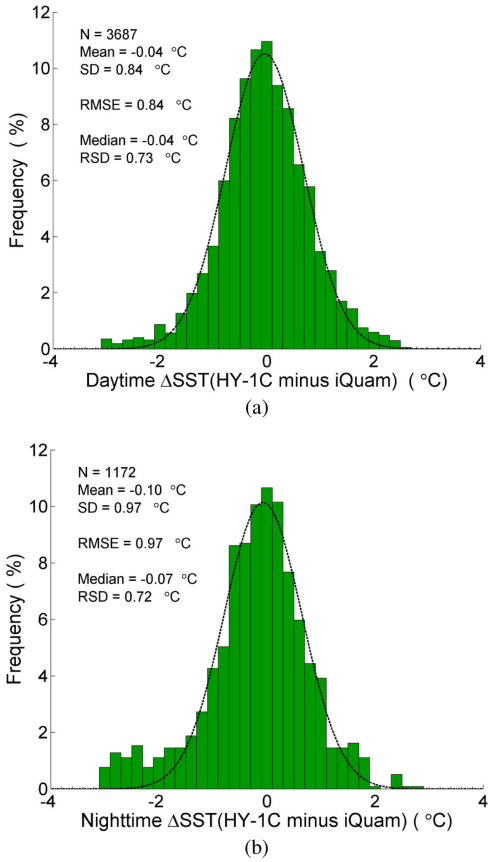

Fig. 4. Histograms of the SST differences between the COCTS and *in situ* measurements from iQuam during (a) daytime and (b) nighttime in the period from January 1, 2019 to March 31, 2020. The dotted black lines in the figures represent the line of probability density function fitting of the Gaussian distribution with a mean of the median and a variance in RSD^2.

TABLE IV
STATISTICS BETWEEN SSTS RETRIEVED FROM COCTS AND *IN SITU* MEASUREMENTS FROM IQUAM

	N	Mean bias (°C)	SD (°C)	RMSE (°C)	Median (°C)	RSD (°C)
Daytime	3687	-0.04	0.84	0.84	-0.04	0.73
Nighttime	1172	-0.10	0.97	0.97	-0.07	0.72

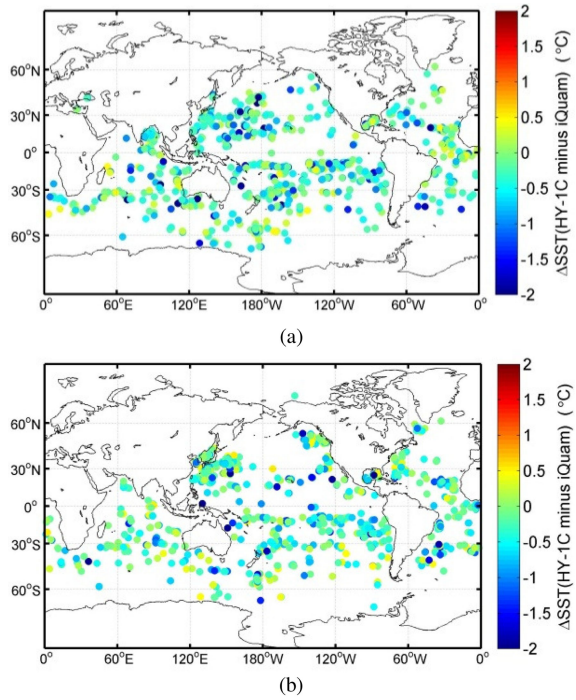

Fig. 5. Locations of the SST differences shown in Fig. 4 for (a) daytime and (b) nighttime.

The median and RSD used can be derived from these difference data by the probability density function fitting of the Gaussian distribution [29].

1) Comparison With in situ *Measurements:* The *in situ* SSTs used for validation in this study are also the ocean water bulk temperatures from the iQuam. Only the *in situ* SSTs with the highest quality (i.e., quality flags of 5 in the dataset) and measured at a water depth of less than 1 m are selected for validation. The time interval between *in situ* and satellite measurements is $\leq$2 h, and the distances between the locations of *in situ* measurements and the nearest clear-sky pixel are $\leq$10 km for validation matchups. The histograms of the SST differences between the COCTS and *in situ* measurements from iQuam in both daytime and nighttime in the period from January 1, 2019 to March 31, 2020 are presented in Fig. 4. The histograms shown in both Fig. 4(a) and (b) have a quasi-Gaussian shape, and they are fitted by the probability density function of the Gaussian distribution to derive the median and RSD; see the dotted black lines in the figures.

The statistics of the mean bias, SD, RMSE, median, and RSD are all presented in Fig. 4. The *N* shown in the figure is the number of data matchups. The mean biases (i.e., the mean shown in Fig. 4), SDs, RMSEs, medians, and RSDs of the daytime and nighttime SSTs retrieved from the COCTS compared with the iQuam data are also detailed in Table IV.

In Fig. 4 and Table IV, the absolutes of the mean bias and medians are not greater than 0.10 °C, the RMSEs are 0.84 and 0.97 °C for daytime and nighttime, the RSDs are 0.73 and 0.72 °C for daytime and nighttime, respectively. The RMSEs and RSDs neither are greater than 1.0 °C.

The locations of the SST differences are shown in Fig. 5, and the comparisons of SST scatterplots from COCTS with the *in situ* measurements from iQuam are shown in Fig. 6.

In Fig. 5(a) and (b), it is shown that the values of the SSTs differences (for both daytime and nighttime) validated against *in situ* measurements from iQuam are distributed in the global ocean with no outstanding geographic distribution characteristics. The SST retrieval method used in this study has the same accuracy for global ocean surfaces. In Fig. 6(a) (daytime) and (b) (nighttime), the scatterplots are distributed uniformly in the ranges from 0 to 30 °C for daytime and 0 to 32 °C for nighttime. The validation results presented in Fig. 4(a) and (b) and Table IV are realistic for the SSTs in their reasonable ranges.

2) Comparison With MODIS Observations: Because the overpass times are similar to those of the descending and ascending nodes for the HY-1C and Terra satellites, the consistency of

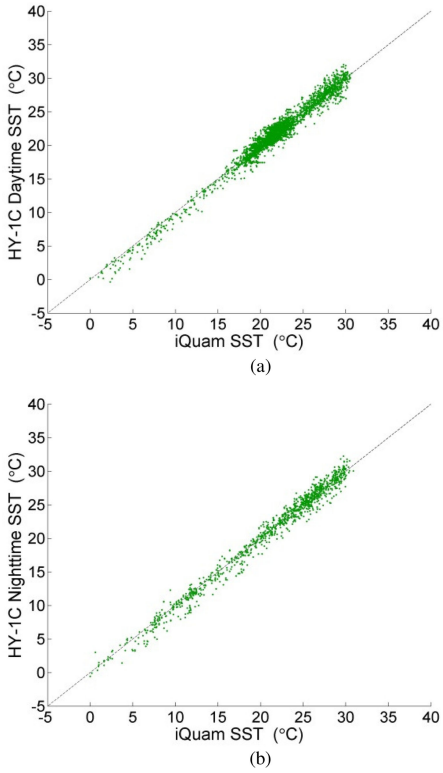

Fig. 6. Comparisons of SST scatterplots from COCTS with the *in situ* measurements from iQuam in (a) daytime and (b) nighttime during the period from January 1, 2019 to March 31, 2020.

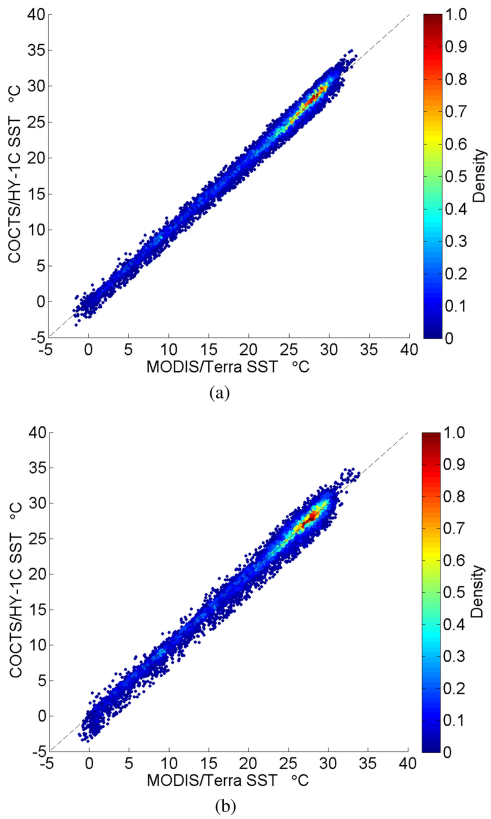

Fig. 7. Comparisons of the density scatterplots of the daily global SSTs between COCTS/HY-1C and MODIS/Terra acquired during (a) daytime and (b) nighttime on October 8, 2019.

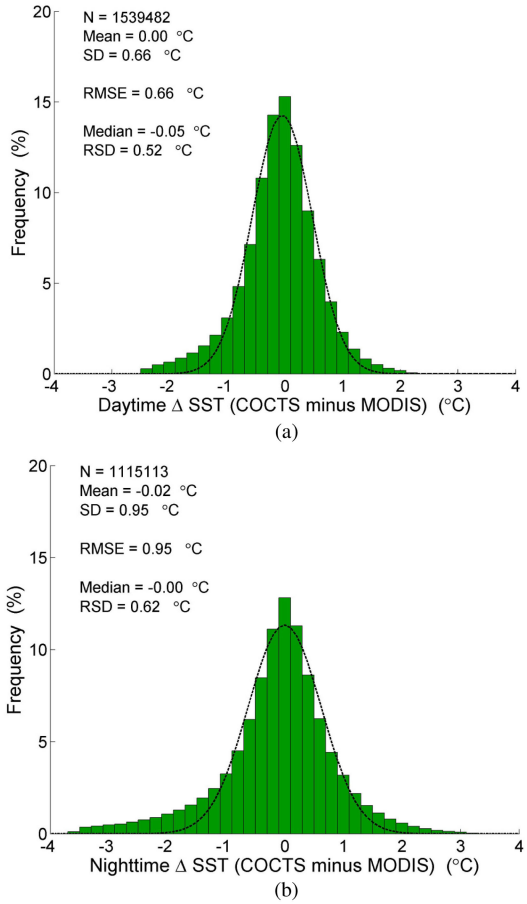

Fig. 8. Histograms of the SST differences between COCTS/HY-1C and MODIS/Terra during (a) daytime and (b) nighttime on October 8, 2019. The dotted black lines in the figures represent the line of probability density function fitting of the Gaussian distribution with a mean of the median and a variance in RSD^2.

SSTs from COCTS/HY-1C and MODIS/Terra can be evaluated by comparing their nearly simultaneous observations. In this study, the daily gridded SST products from the COCTS with a gridded size of 9.2 km are compared with NASA's standard map (L3M) SST products, e.g., the products shown in Figs. 2(a) and 3(a) for COCTS and Figs. 2(b) and 3(b) for MODIS/Terra.

Fig. 7 shows the comparison of COCTS SST scatterplots with those of MODIS during both daytime and nighttime on October 8, 2019, as case studies. Fig. 8 shows the histograms of the SST differences shown in Fig. 7. The daytime SSTs used for comparison in Figs. 7(a) and 8(a) are the data shown in Fig. 2(a) and (b), while the nighttime SSTs compared in Figs. 7(b) and 8(b) are the data shown in Fig. 3(a) and (b). The statistics of the mean bias, SD, RMSE, median, and RSD are all presented in Fig. 8(a) and (b).

Figs. 7 and 8 show that the SSTs from COCTS are consistent with those from MODIS, with mean biases and medians of approximately zero, RMSEs of no greater than 0.66 °C for daytime and 0.95 °C for nighttime, and RSDs of 0.52 °C for daytime and 0.62 °C for nighttime, respectively. For the time series retrieval results from September 10, 2018 to March 31, 2020, Fig. 9

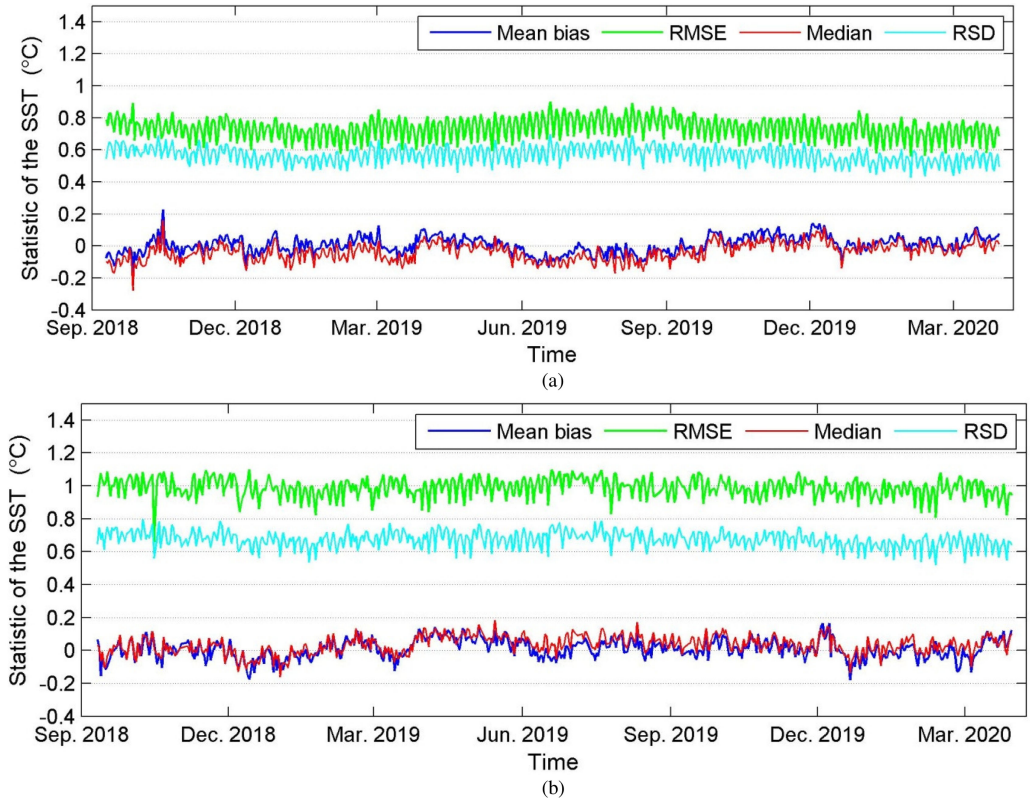

Fig. 9. Comparisons of the global daily gridded SST from COCTS/HY-1C with MODIS/Terra from September 10, 2018 to March 31, 2020 for (a) daytime and (b) nighttime.

TABLE V
STATISTICS (MEAN ± SD) OF THE SST FROM COCTS/HY-1C AGAINST MODIS/TERRA IN A TIME PERIOD FROM SEPTEMBER 10, 2018 TO MARCH 31, 2020

	Mean bias (°C)	RMSE (°C)	Median (°C)	RSD (°C)
Daytime	0.01±0.05	0.73±0.07	-0.04±0.06	0.56±0.05
Nighttime	0.01±0.06	0.99±0.06	0.03±0.06	0.67±0.05

plots the time series of daily mean bias, RMSE, median, and RSD of global daily gridded SST from COCTS/HY-1C minus MODIS/Terra products. The calculation method of the statistics shown in Fig. 9 for each day is the same as that of Figs. 7 and 8.

Fig. 9(a) and (b) shows that the lines of the statistics of both daytime and nighttime SSTs from COCTS are stable over time. The statistics (mean ± SD) of the daily mean biases, RMSEs, medians, and RSDs shown in Fig. 9 are detailed in Table V.

As shown in Fig. 9 and listed in Table V, the means of daily mean biases for more than 18 months from September 10, 2018 to March 31, 2020 are 0.01 ± 0.05 °C for daytime SST and 0.01 ± 0.06 °C for nighttime SST. The means of daily RMSEs are 0.73 ± 0.07 °C for daytime SST and 0.99 ± 0.06 °C for nighttime SST. Both daytime and nighttime SSTs from COCTS are consistent with those from MODIS/Terra.

V. DISCUSSION

Conventional statistics (i.e., mean ± SD or RMSE) are considered to be informative of the performance of the entire SST processing, including the effects of imperfect cloud screening and the sensitivity of the retrieval method to residual unscreened cloud contamination [29].The RMSEs presented in Figs. 4 and 9 and Tables IV and V show that the performance of the daytime SST is better than that of the nighttime SST. The RMSEs of SST from COCTS compared with *in situ* measurements from iQuam are 0.84 °C for daytime and 0.97 °C for nighttime, respectively. The cause of this difference is because the radiances of the first and eighth bands of COCTS/HY-1C in the daytime are used to improve the performance of clear-sky detection. It means that better clear-sky mask algorithms for COCTS are needed in the further, especially for nighttime.

It is noted that the number of nighttime validation matchups is only about one-third of daytime; see the number presented in Fig. 4. The *in situ* data from iQuam with the highest quality (i.e., the quality flags of 5 in the dataset) and measured at a water depth of less than 1 m are selected for validation. After the selection, the *in situ* data used during nighttime are much less than that during daytime.

The median and RSD used in this study are derived from the difference data of the COCTS SST minus *in situ* measurements from iQuam or MODIS SST by the probability density function of the Gaussian distribution fitting. Assuming that the cloud screening is fairly efficient (i.e., that the majority of data are indeed cloud free), the robust statistics (i.e., the median and RSD) more fairly characterize the performance of the retrieval method itself when applied to the clear-sky data for which it is truly intended [29]. In Tables IV and V, 1) the values of RSDs

are smaller than their corresponding RMSEs, and 2) the RSDs of daytime SSTs are almost the same as those of nighttime SSTs. There is some residual unscreened cloud contamination in the clear-sky/cloud mask processing (see the data on the left side of Fig. 4(b), i.e., the data smaller than -2 °C) and the RSDs of the SST retrieval algorithms for the clear-sky COCTS data used in this study are $\sim$0.70 °C during both daytime and nighttime.

VI. Conclusion

The COCTS onboard the HY-1C satellite is designed for global SST and ocean color detection. Both daytime and nighttime SSTs are derived from the BTs of the two TIR bands at 10.8 and 12.0 μm of COCTS by the NLSST algorithm. The SST retrieval results from the MCSST algorithm are used as the first guess for the input of the NLSST algorithm in this study. The SST retrieval results of this study show that the COCTS can detect the global SST twice a day (once during daytime and once at nighttime).

The comparison of the SST from COCTS/HY-1C with *in situ* measurements from iQuam during the period from January 1, 2019 to March 31, 2020 shows that the RMSEs are 0.84 °C for daytime and 0.97 °C for nighttime, and the RSD are 0.73 °C for daytime and 0.72 °C for nighttime, respectively. A comparison of the SST from COCTS with MODIS during the period from September 10, 2018 to March 31, 2020 shows that both daytime and nighttime COCTS SSTs are consistent with MODIS/Terra SSTs. The COCTS sensor has a satisfactory performance for global SST observations, and the SST retrieval method and processing used in this study work well.

Differences may exist among SST product versions, which are computed by different SST retrieval algorithms with coefficients regressed by different matchups between satellite observations and *in situ* measurements. The SSTs from COCTS/HY-1C presented and evaluated here are computed by the algorithms developed in this study, and they are the preliminary analysis. More detailed analyses and evaluations will be considered in future investigations.

Acknowledgment

The authors would like to thank NASA Godard Space Flight Center, Ocean Ecology Laboratory, and Ocean Biology Processing Group (OBPG) for providing access to the MODIS/Terra data, as well as the Center for STAR and NOAA Satellite and Information Service (NESDIS) for providing access to the *in situ* data of iQuam.

References

[1] C. C. Walton, W. G. Pichel, J. F. Sapper, and D. A. May, "The development and operational application of nonlinear algorithms for the measurement of sea surface temperatures with the NOAA polar-orbiting environmental satellites," *J. Geophys. Res.*, vol. 103, no. C12, pp. 27999–28012, Nov. 1998.

[2] F. J. Wentz, C. Gentemann, D. Smith, and D. Chelton, "Satellite measurements of sea surface temperature through clouds," *Science*, vol. 288, pp. 847–850, May 2000.

[3] R. W. Reynolds, N. A. Rayner, T. M. Smith, D. C. Stokes, and W. Wang, "An improved in situ and satellite SST analysis for climate," *J. Clim.*, vol. 15, pp. 1609–1625, Jul. 2002.

[4] C. Donlon *et al.*, "The global ocean data assimilation experiment high-resolution sea surface temperature pilot project," *Bull. Amer. Meteorol. Soc.*, pp. 1197–1213, Aug. 2007.

[5] M. Manzano-Sarabia, C. A. Salinas-Zavala, M. Kahru, S. E. Lluch-Cota, and A. Gonzaález-Becerril, "The impact of the 1997–1999 warm-SST and low-productivity episode on fisheries in the southwestern Gulf of Mexico," *Hydrobiologia*, vol. 610, no. 1, pp. 257–267, 2008.

[6] C. Paulino, M. Segura, and G. Chacón, "Spatial variability of jumbo flying squid (*Dosidicus gigas*) fishery related to remotely sensed SST and chlorophyll-a concentration (2004–2012)," *Fish. Res.*, vol. 173, no. Part 2, pp. 122–127, Jan. 2016.

[7] V. Banzon, T. M. Smith, T. M. Chin, C. Liu, and W. Hankins, "A long-term record of blended satellite and in situ sea-surface temperature for climate monitoring, modeling and environmental studies," *Earth Syst. Sci. Data*, vol. 8, pp. 165–176, 2016.

[8] P. Chan and B. Gao, "A comparison of MODIS, NCEP, and TMI sea surface temperature datasets," *IEEE Geosci. Remote Sens. Lett.*, vol. 2, no. 3, pp. 270–274, Jul. 2005.

[9] E. P. Mcclain, W. G. Pichel, C. C Walton, Z. Ahmad, J. Sutton, P. Mcclain, W. G. Pichel, and C. C. Walton, "Multi-channel improvements to satellite-derived global sea surface temperatures," *Adv. Space Res.*, vol. 2, no. 6, pp. 43–47, 1982.

[10] E. P Mcclain, W. G. Pichel, and C. C. Walton, "Comparative performance of AVHRR-based multichannel sea surface temperatures," *J. Geophys. Res.-Oceans.*, vol. 90, no. C6, pp. 11587–11601, Nov. 1985.

[11] P. L. Le Borgne, H. Roquet, and C. J. Merchant, "Estimation of sea surface temperature from the Spinning Enhanced Visible and Infrared Imager, improved using numerical weather prediction," *Remote Sens. Environ.*, vol. 115, pp. 55–65, 2011.

[12] B. Petrenko, A. Ignatov, N. Shabanov, and Y. Kihai, "Development and evaluation of SST algorithms for GOES-R ABI using MSG SEVIRI as a proxy," *Remote Sens. Environ.*, vol. 115, pp. 3647–3658, 2011.

[13] B. Petrenko, A. Ignatov, Y. Kihai, J. Stroup, and P. Dash, "Evaluation and selection of SST regressing algorithms for JPSS VIIRS," *J. Geophys. Res. Atmos.*, vol. 119, pp. 4580–4599, Apr. 2014.

[14] B. Ai, Z. Wen, Y. Jiang, S. Gao, and G. Lv, "Sea surface temperature inversion model for infrared remote sensing images based on deep neural network," *Infrared Phys. Technol.*, vol. 99, pp. 231–239, 2019.

[15] K. A. Kilpatrick, G. P. Podestá, and R. Evans, "Overview of the NOAA/NASA advanced very high resolution radiometer Pathfinder algorithm for sea surface temperature and associated matchup database," *J. Geophys. Res.*, vol. 106, no. C5, pp. 9179–9197, May 2001.

[16] K. A. Kilpatrick *et al.*, "A decade of sea surface temperature from MODIS," *Remote Sens. Environ.*, vol. 165, pp. 27–41, 2015.

[17] K. Hosoda and H. Qin, "Algorithm for estimating sea surface temperatures based on Aqua/MODIS global ocean data. 1. Development and validation of the algorithm," *J. Oceanogr.*, vol. 67, pp. 135–145, Feb. 2011.

[18] K. Hosoda, H. Murakami, F. Sakaida, and H. Kawamura, "Algorithm and validation of sea surface temperature observation using MODIS sensors aboard Terra and Aqua in the Western North Pacific," *J. Oceanogr.*, vol. 63, pp. 267–280, 2007.

[19] R. F. Vincent, R. F. Marsden, P. J. Minnett, K. A. M. Creber, and J. R. Buckley, "Arctic waters and marginal ice zones: A composite Arctic sea surface temperature algorithm using satellite thermal data," *J. Geophys. Res.*, vol. 113, 2008, Art. no. C04021.

[20] R. M. Vavalli, "Retrieval of sea surface temperature from MODIS data in coastal water," *Sustainability*, vol. 9, Nov. 2017, Art. no. 2032.

[21] Q. Song *et al.*, "Vicarious calibration of COCTS-HY-1C at visible and near-infrared bands for ocean color application," *Opt. Exp.*, vol. 27, no. 20, pp. 1615–1626, Sep. 2019.

[22] C. J. Donlon *et al.*, "Toward improved validation of satellite sea surface skin temperature measurements for climate research," *J. Clim.*, vol. 15, pp. 353–369, Feb. 2002.

[23] P. J. Minnett, "Radiometric measurements of the sea-surface skin temperature: The competing roles of the diurnal thermocline and the cool skin," *Int. J. Remote Sens.*, vol. 24, no. 24, pp. 5033–5047, 2003.

[24] O. B. Brown and P. J. Minnett, "MODIS infrared sea surface temperature algorithm—Algorithm theoretical basis document (version 2.0)," Univ. Miami, Miami, FL, USA, Tech. Rep. NAS5-31361, Apr. 1999.

[25] B. Petrenko and J. Stroup, "Advanced clear-sky processor for oceans (ACSPO)-VIIRS, algorithm theoretical basis document, version 1.0," SST Integrated Product Team (IPT), NPOESS Data Exploitation Project (NDE), and Office of Satellite and Product Operations (OSPO), USA, Aug. 2013. [Online]. Available: https://www.star.nesdis.noaa.gov/jpss/documents/ATBD/ATBD_ACSPO_SST_v1.0.pdf

[26] F. Xu and A. Ignatov, "In-situ SST quality monitor (iQuam)," *J. Atmos. Ocean. Technol.*, vol. 31, pp. 164–180, Feb. 2014.
[27] J. W. Campbell, J. M. Blaisdell, and M. Darzi, "Level-3 SeaWiFS data products: Spatial and temporal binning algorithms," in *NASA Tech. Memo. 104566*, vol. 32, S. B. Hooker, E. R. Firestone, and J. G. Acker, Eds., Greenbelt, MD, USA: NASA Goddard Space Flight Center, 1995.
[28] C. J. Marchant and A. R. Harris, "Toward the elimination of bias in satellite retrievals of sea surface temperature 2. Comparison with in-situ measurements," *J. Geophys. Res.*, vol. 104, no. C10, pp. 23579–23590, Oct. 1999.
[29] C. J. Merchant, P. Le Borgne, A. Marsouin, and H. Roquet, "Optimal estimation of sea surface temperature from split-window observations," *Remote Sens. Environ.*, vol. 112, pp. 2469–2484, 2008.
[30] H. Wang, L. Guan, and G. Chen, "Evaluation of sea surface temperature from FY-3C VIRR data in the Arctic," *IEEE Geosci. Remote Sens. Lett.*, vol. 13, no. 2, pp. 292–296, Feb. 2016.
[31] M. Yang, L. Guan, H. Beggs, N. Morgan, Y. K. Urihara, and M. Kachi, "Comparison of Himawari-8 AHI SST with shipboard skin SST measurements in the Australian region," *Remote Sens.*, vol. 12, Apr. 2020, Art. no. 1237.

Xiaomin Ye received the B.S. degree in optical information science and technology from Nankai University, Tianjin, China, in 2006, the master's degree in physical oceanography from the First Institute of Oceanography, State Oceanic Administration, Qingdao, China, in 2009, and the Ph.D. degree in oceanic detection technology from the Ocean University of China, Qingdao, China, in 2017.

He is currently a Designer-in-Charge of data processing for the Chinese HY-1C/D satellite with National Satellite Ocean Application Service, Beijing, China. His research interests include electromagnetic wave scattering from the ocean surface and the application of ocean satellite data.

Jianqiang Liu received the B.S. degree in geophysics from Peking University, Beijing, China, in 1986 and the master's degree in marine meteorology from National Marine Environmental Forecasting Center, State Oceanic Administration, Beijing, China, in 1989.

He is the Chief Designer of the ground application system for Chinese−France Ocean Satellite and new generational ocean color satellites, and was a Deputy Chief Designer of the ground application system for HY-1 and HY-2 satellites. He is one of the founders of Satellite Ocean Remote Sensing in China and plays an important role in the development of Chinese Ocean Satellite and Manned Space Flight. His research interests include ocean color and sea wave satellite data processing, applications of ocean remote sensing data, and Antarctic research.

Mingsen Lin (Member, IEEE) received the B.S. degree in applied mechanics from National University of Defense Technology, Changsha, China, in 1984, and the Ph.D. degree in computational mathematics from the Computing Center, Chinese Academy of Sciences, Beijing, China, in 1992.

He is the Chief Designer of the ground application system for Chinese salinity satellites, synthetic aperture radar satellites, and new generational ocean dynamic satellites, and also was a Deputy Chief Designer of the ground application system for HY-1 and HY-2 satellites, where he organized the framework for the Chinese Ocean Satellite outline and managed the construction of the ground application system for the Chinese Ocean Satellite with National Satellite Ocean Application Service, Beijing, China. He is one of the founders of Satellite Ocean Remote Sensing in China. He plays an important role in the development of Chinese ocean satellite and manned space flight. His research interests include ocean satellite data processing and remote sensing of the ocean and their applications.

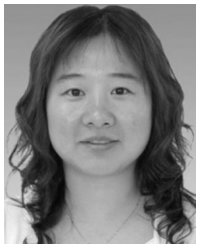

Jing Ding received the Ph.D. degree in physical oceanography from Ocean University of China, Qingdao, China, in 2004.

She has always focused on ocean color remote sensing and satellite data processing. She has been with NSOAS since 2004, where she has been a Research Scientist in areas of satellite remote sensing, especially in satellite projects for ocean color and coastal environment monitoring. Currently, she is the Head of HY-1C/D satellite data processing group involved in the strategy and framework for satellite data processing as well as the algorithms related with ocean color products and applications.

Bin Zou received the B.S. degree in meteorology from Peking University, Beijing, China, in 1992, and the master's degree in marine meteorology from National Marine Environmental Forecasting Center, State Oceanic Administration, Beijing, China, in 1995.

He is a Deputy Chief Designer of the ground application system for HY-1C/D satellites. He has been to Antarctica, in 1995 for Antarctic sea ice monitoring, research, and application and to Arctic, in 1999 for Arctic sea ice and sea fog research. Currently, he is engaged in ocean remote sensing, satellite ground data processing system construction technology, ocean color satellite product processing algorithm and software, ocean oil spill monitoring, and remote sensing fishery application.

Qingjun Song received the B.S. degree in applied physics from the Hefei University of Technology, Hefei, China, in 2001, and the M.S. degree in ocean technology from Dalian Ocean University, Dalian, China, in 2012.

He is currently a Researcher with the National Satellite Ocean Application Service, Ministry of Natural Resources, Beijing, China, and works on HY-1 and HY-2 series satellite instruments calibration and ocean remote sensing products validation. His research interests include remote sensing and the absolute radiometric calibration of optical instruments.